Open Access

High-Power (>300 mW) On-Chip Laser With Passively Aligned Silicon-Nitride Waveguide DBR Cavity

Volume 12, Number 6, December 2020

Dave Kharas, *Member, IEEE*
Jason J. Plant
William Loh
Reuel B. Swint
Suraj Bramhavar
Christopher Heidelberger
Siva Yegnanarayanan
Paul W. Juodawlkis, *Fellow, IEEE*

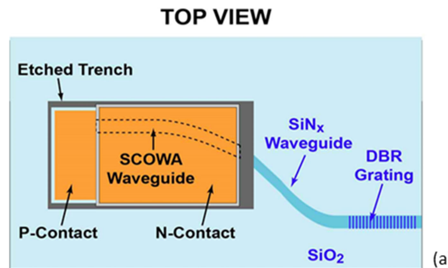

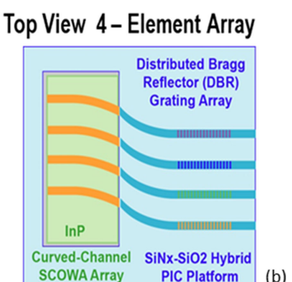

DOI: 10.1109/JPHOT.2020.3037834

High-Power (>300 mW) On-Chip Laser With Passively Aligned Silicon-Nitride Waveguide DBR Cavity

Dave Kharas, *Member, IEEE*, Jason J. Plant, William Loh, Reuel B. Swint, Suraj Bramhavar, Christopher Heidelberger, Siva Yegnanarayanan, and Paul W. Juodawlkis, *Fellow, IEEE*

Massachusetts Institute of Technology (MIT) Lincoln Laboratory, Lexington, MA 02420 USA

DOI:10.1109/JPHOT.2020.3037834
This work is licensed under a Creative Commons Attribution 4.0 License. For more information, see https://creativecommons.org/licenses/by/4.0/

Manuscript received November 6, 2020; accepted November 9, 2020. Date of publication November 16, 2020; date of current version December 2, 2020. This work was supported by the United States Air Force under Air Force Contract FA8702-15-D-0001. Any opinions, findings, conclusions or recommendations expressed in this material are those of the author(s) and do not necessarily reflect the views of the United States Air Force. Corresponding author: Dave Kharas (e-mail: Dave.Kharas@ll.mit.edu).

Abstract: We demonstrate a high-power on-chip 1550-nm laser implemented by passive flip-chip integration of a curved-channel, double-pass InGaAsP/InP slab-coupled optical waveguide amplifier (SCOWA) onto a photonic integrated circuit (PIC) containing a silicon nitride (SiN) waveguide and distributed Bragg reflector (DBR) grating. The combined chip-scale SCOW external cavity laser (SCOWECL) has single mode emission with 312 mW of optical power at a drive current of 2.5 A, and exhibits a side mode suppression ratio (SMSR) of 55 dB, peak photon conversion efficiency (PCE) of 10%, low relative-intensity noise (RIN) of ~160 dB/Hz, and an integrated linewidth of 192 kHz. Additionally, we demonstrate a multi-wavelength SCOWECL array comprised of four SCOWAs coupled to SiN-waveguide DBR gratings. The four-element array generates 80 mW per channel when the SCOWAs are driven in parallel (1.25 A/channel) with ~1-nm wavelength spacing centered at 1533 nm. We describe the fabrication and hybrid integration processes. The measured SCOWA-to-waveguide coupling loss is estimated to be 1.6 +/−1.0 dB which agrees well with the simulation.

Index Terms: Hybrid integration, SiN photonics, external cavity laser, high power laser.

1. Introduction

Photonic integrated circuits (PICs) utilizing silicon or silicon nitride (SiN) waveguides have gained prominence as the leading photonic platforms to support a wide variety on-chip optical processing applications. For applications requiring manipulation of wavelengths outside the telecom regime (<1.1 μm) or higher optical powers (>100 mW) where silicon begins to suffer from increased optical loss due to two-photon absorption (TPA), SiN waveguides are preferred [1]. In both PIC waveguide systems, there is a lack of availability of a native light source, requiring integration of light emitters fabricated from direct bandgap materials. The most mature integration paths either employ heterogeneous III-V epitaxial material transfer that is evanescently coupled to PIC substrates [2]–[6], or hybrid approaches where completed best-of breed devices are flip-chip bonded or butt-coupled directly to the PIC [7]–[14]. High brightness, narrow linewidth, low noise laser sources are particularly desirable for microwave photonics (MWP) and optical beam forming applications.

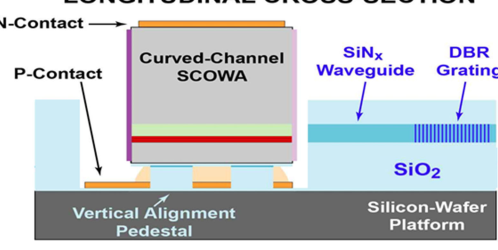

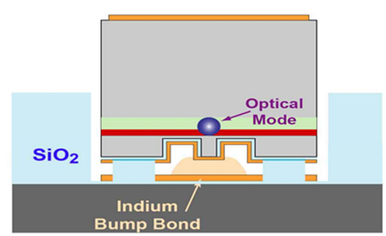

Fig. 1. (a) Diagram of the top view of a single element and (b) 4-element SCOWA device hybridized in a photonic submount with SiN waveguides and DBR gratings. Schematics of (c) longitudinal and (d) transverse cross-sections of the single-element device architecture.

Among the choices of III-V waveguide emitter architectures, slab-coupled optical waveguide amplifiers (SCOWAs) are particularly well suited to hybrid integration due to their capability for high optical power emission, and large ($\sim 5 \times 8$ μm) mode size which reduces coupling sensitivity to waveguide misalignment [15], [16]. In this study, we describe development of a high power external-cavity laser (ECL) that is formed by hybrid integration of an 8-mm-long double-pass InGaAsP/InP SCOWA with a low-loss (0.2 dB/cm) SiN waveguide [1] containing a 18-mm-long distributed Bragg reflector (DBR) grating. The hybrid integration is accomplished by the fabrication of a photonic multi-chip module submount featuring a SiN waveguide that is encapsulated in a thick silicon oxide cladding layer. We etch an insert slot into the oxide surface to accommodate the SCOWA device. The insert location features pedestals that support the SCOWA chip and provide for vertical alignment, and a bottom electrode pad and indium bumps for flip chip soldering of our SCOWA device. A schematic representation of the integration approach is shown in Fig 1.

In this work we describe the fabrication process for the photonic multi-chip module, the SCOWA device, and the hybridization process employed. We then report on the operation of single and 4-element SCOWECL devices, and the measurement of their optical performance. Additionally we estimate the coupling loss between the SCOWA device and PIC and compare it to a finite-difference time-domain (FDTD) simulation of coupling loss.

2. Device Fabrication

2.1 Photonic Multi-Chip Module Submount

The SiN PIC photonic multi-chip module submount fabrication is carried out in MIT Lincoln Laboratory's (LL) Microelectronic Laboratory (ML) which contains a 200 mm, 90-nm node silicon fabrication toolset. The process flow (see Fig. 2) starts with deposition of a 7.5-μm-thick silicon dioxide (SiO_2) layer by plasma-enhanced chemical vapor deposition (PECVD), which acts as the bottom cladding layer for the waveguide. The oxide layer is annealed at 1100°C to reduce hydrogen content, which reduces optical loss. The final lower-cladding oxide thickness is set by a chemo-mechanical polish (CMP) step, with the deposition and polish thickness target determined to ensure that the waveguide center line is matched to the position of the optical mode center in the

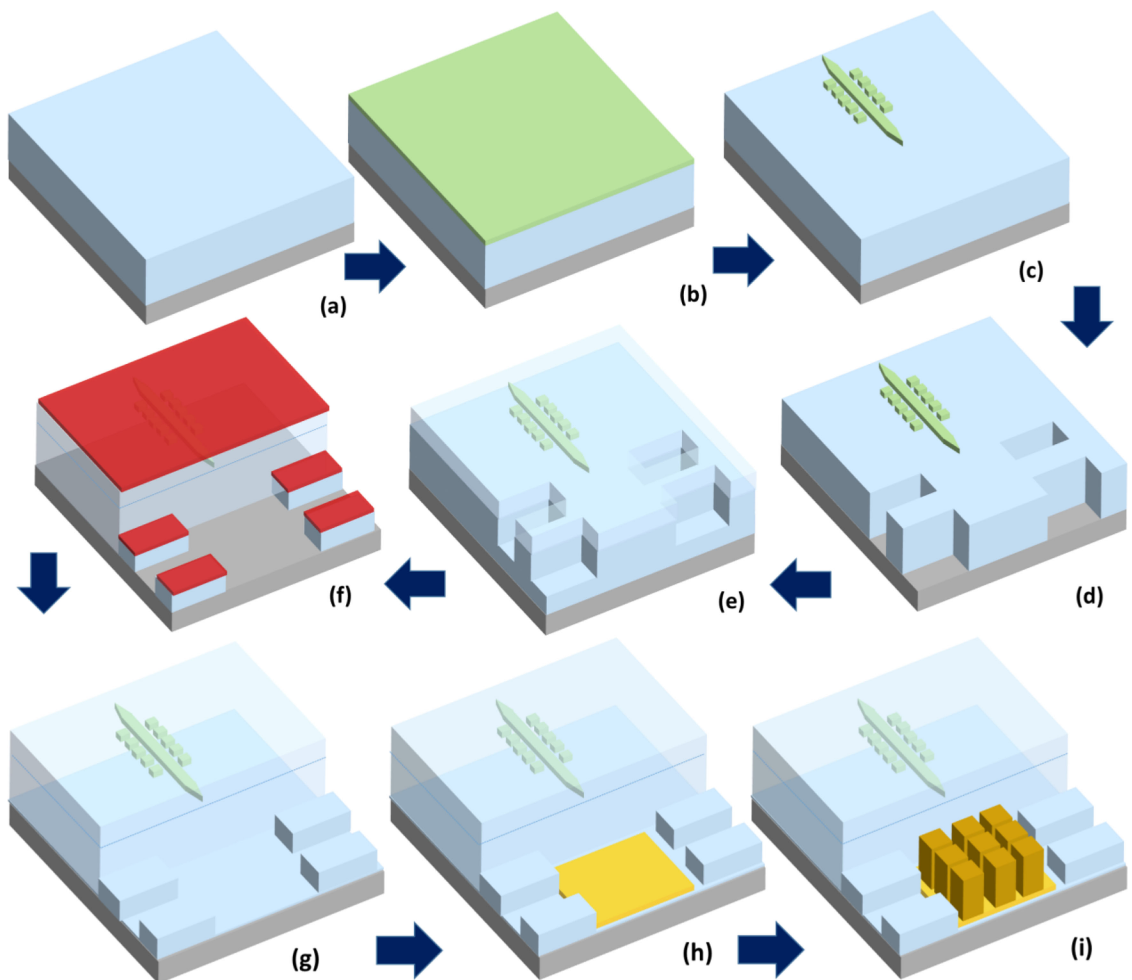

Fig. 2. Fabrication flow for the photonic multi-chip module submount, illustrating, (a) initial oxide bottom clad deposition, (b) LPCVD SiN waveguide layer deposition, (c) waveguide, DBR, and mode converter patterning, (d) trench etch for vertical-alignment pedestals, (e) oxide deposition for the top clad, and vertical-alignment pedestals, (f) resist masking and insert-slot trench etch (oxide boundary marked by dotted line), (g) passivation oxide deposition, (h) metal bond pad evaporation and liftoff, (i) indium solder bump array evaporation and liftoff.

flip-chip bonded SCOWA. The waveguide and gratings are formed in a 200-nm-thick low pressure chemical vapor deposition (LPCVD) stoichiometric Si_3N_4 that is patterned using an ASML 193-nm stepper and etched by a SF_6 based plasma-etch chemistry. The SiN waveguide terminates at both the chip edge and at the SCOWA insert location with inverse linear tapers 500 μm in length and 0.45 μm tip width that increase the optical mode size from $\sim$1.4 μm (lateral) $\times$ 0.9 μm (vertical) to $\sim$5.0 μm $\times$ 4 μm 1/e^2-mode-field diameter. The expanded mode provides for good matching to a lensed polarization-maintaining fiber having a 6.5-μm spot size, and to the SCOWA mode, which measures 8 μm (lateral) $\times$ 5 μm (vertical) in size. The simulated and measured mode profiles as well as an assessment of the SCOWA-to-SiN-waveguide coupling efficiency are presented in Sections 3.1 and 3.3, respectively. The DBR grating utilized is a low kappa design similar to that described by Spencer *et al.* [14] consisting of an 18-mm-long array of 200-nm diameter posts set at a 508-nm pitch and spaced at a separation gap of 1.2 μm positioned on either side of a 1.1-μm wide SiN waveguide. The waveguide grating has a measured reflectivity of $\sim$20% with a measured bandwidth of 0.23 nm.

After the waveguides and DBR gratings are etched, trenches to define the vertical-alignment pedestal regions are lithographically patterned and etched through the bottom oxide to the silicon substrate surface. A 3.0-μm-thick PECVD oxide is then deposited, which serves as both a top cladding layer for the SiN waveguide and the vertical-alignment pedestal layer. The wafer is coated in resist and a 3 mm $\times$ 8 mm region is opened to define the insert slot location for the III-V flip-chip die attach. The surrounding upper-cladding regions and the oxide inside the vertical-alignment trenches are protected by resist during the 10.5-μm deep insert slot etch. After resist strip, we are left with 3.0-μm-tall vertical-alignment pedestals that will support the III-V flip-chipped device and provide the vertical registration between the SCOWA waveguide region and the SiN waveguide. This approach to fabricating the vertical-alignment pedestals allows them to be formed from the more accurate PECVD oxide-deposition process, rather than by a less uniform timed etch into the oxide stack.

Once the insert region is opened, a 100 nm thick PECVD oxide passivation layer is deposited into the insert slot to provide electrical isolation from the semi-insulating silicon substrate. An electrical contact pad metal consisting of a stack of Ti/Al/Ti/Pt/Au (nominally 500-nm thick) is created by evaporation and liftoff into the bottom of the insert region. An array of 15-μm wide and 6.5-μm tall indium bumps are similarly formed on top of the contact pad by evaporation and liftoff. The bump array is laid out on a 32-μm pitch, with the intent to achieve a fill factor of $\sim$70% after compression. During flip chip bonding the bump array is compressed to a thickness of $\sim$2 μm. Analysis of parts that were mechanically separated after bonding showed an indium adhesion footprint more indicative of a fill factor closer to 50-60%, which is a result of the reduced indium bump volume from the pyramidal shapes of the bumps formed during the liftoff process. The choice of indium as a bond metal is driven primarily by experience on other programs at Lincoln Laboratory, and the use of more reliable solder systems such as AuSn is of interest for future study.

The fabrication flow is illustrated in Fig. 2, and images of the completed submount and SCOWA devices are shown in Fig. 3. The photonic submount chip measures 26 mm $\times$ 32 mm, and contains 14 insert slot locations with a variety of grating designs for both single and 4-element SCOWA hybridization. The insert slots designed for coupling to the 4-element SCOWA featured 4 waveguides with DBR gratings having varying pitch to create emission on a 1-nm wavelength spacing.

2.2 SCOWA Device Fabrication

The InGaAsP/InP SCOWA devices are fabricated in MIT LL's Compound Semiconductor Laboratory (CSL), which encompasses both epitaxial growth and wafer processing capabilities. The amplifiers were grown via organo-metallic vapor-phase epitaxy (OMVPE) on n-type (100) 2" diameter InP substrates. The material structure consists of n-InP buffer and lower-cladding layers, a thick (4.6 μm) InGaAsP waveguide layer (bandgap 1.2 eV), three 8-nm-thick compressively strained (1%) InGaAsP quantum wells with 10-nm-thick tensile-strained barriers, a p-InP upper-cladding layer and a compositionally graded p+ InGaAsP contact layer. Following epi growth the peak photoluminescence wavelength of the active region was measured to be 1.57 μm. The double-pass SCOWAs were fabricated using the process steps outlined in Ref. [15] with either a single 5-μm-wide ridge curved at a 5 degree at the input facet, or a similar device with an array of four ridges spaced 50 μm apart. After fabrication, the bars of devices were mechanically cleaved and facets coated with antireflective (AR) and highly reflective coatings (HR) on the front and rear facets respectively. These bars were then further mechanically cleaved into chips (nominally 8-mm long by 2-mm wide) containing either a single SCOWA or a 4-element array of SCOWAs with a single electrical contact. Images of the SCOWA devices are seen in Fig. 3(b).

2.3 Hybridization

Prior to flip-chip bonding, both the submount and SCOWA devices were cleaned in an atmospheric downstream Ontos plasma system to remove interfacial oxides on the indium surface and any

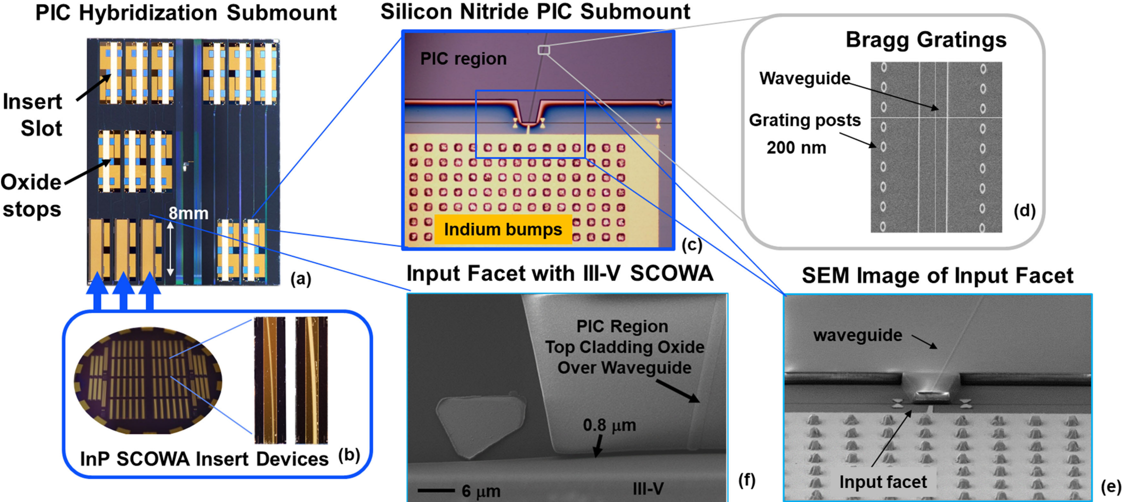

Fig. 3. Optical and SEM images of the fabricated SiN multi-chip photonic submount, SCOWA device, and hybridized regions of the chip. The PIC submount (a) features 14 insert slot locations, with 6 mechanical stops at each insert slot (light blue color). The fabricated SCOWA wafer and a single element and 4-element device are shown (b). Three single-element devices have been flip-chip bonded into the bottom left 3 insert slots of the submount shown in (a). An optical microscope image of the front region of the insert slot (c) shows the bottom P-electrode contact pad, indium solder bump array, and the input facet region. The SiN waveguide is visible (black line) in the oxide region of the PIC (purple region). A SEM image of the DBR grating structure showing 200-nm wide posts, and 1.1-μm wide waveguide (d). A tilted SEM view of the input region is shown in image (e) illustrating the location of waveguide, and the wall of the 10-μm deep insert slot. A top-down SEM image of an insert slot with a SCOWA device flip-chip bonded into position is visible in image (f), here the III-V device has been placed on-top of the indium bump array that was visible in image (d), and the emitting face abuts the input facet region with a 0.8-μm separation gap. The triangular mark on the left side of the image is a fiducial mark to help in aligning the III-V edge with the input facet.

organic contaminants that could hinder attach. Flip-chip bonding was carried out using a commercial SET FC 150 flip-chip bonding system, featuring a high magnification vision system enabling fine alignment of the SCOWA device to fiducial features located on the submount. The chips are first roughly aligned at room temperature. Then, to minimize thermal related shifting, both chips are brought up to a 170°C bonding temperature with a cover flow of N_2 gas, and fine aligned. Because the SCOWA chip dimensions are set by mechanical cleaving, the chip length can vary up to 20 μm from the ideal break line, this variation in the position of the front facet precludes us from using a cross-hair type fiducial mark for aligning the chip both in the forward and lateral directions. Instead we employ long Vernier bars that span the cleave line and are angled at the same 5 degree angle as the waveguide ridge. These are present at the front edge of the SCOWA chip irrespective of where the cleave actually takes place. During alignment, these Vernier marks overlay with matching marks patterned on the pad metal that have a 0.4-μm Vernier constant are used for lateral registration of the SCOWA chip. For forward positioning of the SCOWA chip, a pair of triangular marks with a 1.5-μm gap serve as fiducials for aligning the front facet of the SCOWA device and positioning the SCOWA device into the slot with a 1-2 μm forward offset. Figure 4(a,b) show images captured from the FC 150 microscope showing the SCOWA chip in a green false color overlayed to the gold pad metal alignment fiducials in the insert slot of the submount chip. Once the alignment is optimized, the machine optics are removed from the bonding path, and the SCOWA chip is lowered into position onto the indium bump array inside the insert slot of the submount. A bonding pressure of 1.875 MPa is applied for 60 sec, and then maintained for an additional 180 sec while the stage temperature is cooled down to 70°C. For the work reported here, eight SCOWA devices were flip-chip bonded (4 single element and 4 four-element devices).

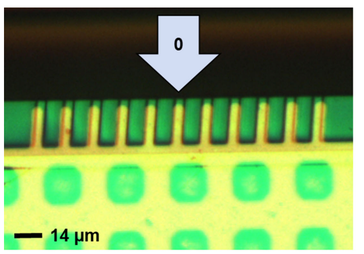

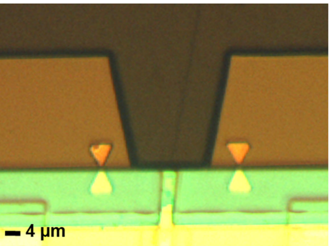

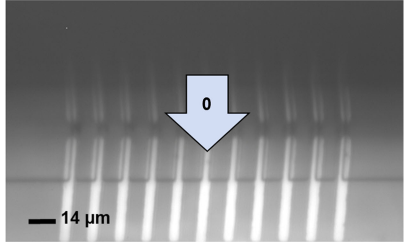

Fig. 4. Optical images of the alignment fiducials of the SCOWA and PIC submount as captured from the SET FC 150 vision system (a) and (b). In image (a) are the Vernier marks used for lateral alignment of the SCOWA chip in green, and the underlying Au marks visible in yellow. The Vernier constant is 0.4 μm allowing us to readily identify shifting left or right up to 2.0 μm, in this image the two chips are aligned and nearly centered with blue arrow marking the centered position. In top half of image (b) the front input facet of the PIC is visible with the SiN waveguide taper visible in the transparent cladding oxide in the trapezoidal shaped input region. In the lower half of the image the 5-μm wide ridge of the SCOWA is seen. The pair of nearly touching Au triangles define a target gap of ~1.5 μm serve as visual markers for aligning the SCOWA front edge (note for the case illustrated here the SCOWA chip is nearly touching the input facet, and would be shifted further down prior to initiating the bond. Image (c) is an IR microscope image of a flip chip bonded device showing centered Vernier marks.

Following insertion, the alignment is verified using an Infrared microscope system consisting of a Hamamatsu InGaAs camera, mounted on a Nikon inspection microscope with 500X objectives achieving a 0.2 μm/pixel resolution. An IR image of the lateral alignment Verniers after bonding is visible in Fig. 4(c). Measurements of stand-off separation, and vertical registration can be determined with top-down, and edge-on scanning electron microscopy (SEM). For these experiments, we are able to obtain a mean positional error in bonding of 1.2 $+/-0.8$ μm in both lateral and stand off directions from the input facet waveguide (placement accuracy within spec of the FC-150). SEM inspection confirmed that the SCOWA chips are sitting in contact with the pedestals ensuring a vertical alignment error of <0.25 μm. For this positional error estimate, an error of zero corresponds to a placement of the SCOWA with the waveguide centerlines perfectly aligned laterally and with no air gap between the SCOWA and the PIC facet. Optical and SEM Images of the hybridized chips can be seen in Fig. 3(a) and in 3(f).

3. Device Characterization

3.1 Laser Testing

Hybridized SCOWECL devices were tested for optical power vs. current and voltage (L-I-V) using an optical probe station with probes placed on the device backside n-contact and a p-contact break-out pad on the photonic submount. Devices were forward biased up to a drive current of 2.5 A for the single-element devices, and to 5 A for the 4-element array. The SCOWAs in the 4-element array are connected in parallel, so each SCOWA is driven at 1.25 A. Devices under test were mounted to a copper heat spreader and connected to a thermoelectric cooler maintaining a temperature of 25.0°C with a thermocouple reading from the center of the copper block. Optical emission from the SiN waveguide output at the chip edge was collected with a 0.55 NA aspherical lens focused onto a powerhead, and the resulting data were corrected for the lens loss (0.7 dB). The L-I curves and wall-plug efficiencies (optical power / electrical power) of 3 single-element SCOWECLs are shown in Fig. 5(a). The best performing device (A) emitted 312 mW at 2.5 A with a peak wall plug efficiency of ~10% at 1-A bias current and had a threshold current of 0.36 A which corresponds to a current density of 900 A/cm^2 in the active region. The two other devices (B,C) having slightly worse placement accuracy emitted approximately 280 mW at the same 2.5-A bias. The L-I performance of a 4-element hybridized laser device is seen in Fig 5(b), which emits 80 mW of power per channel at 1.25-A bias per element. Mode hopping behavior is visible in some of the LIV plots. Given the reflector bandwidth of 0.23 nm and a free spectral range of 0.03 nm, we

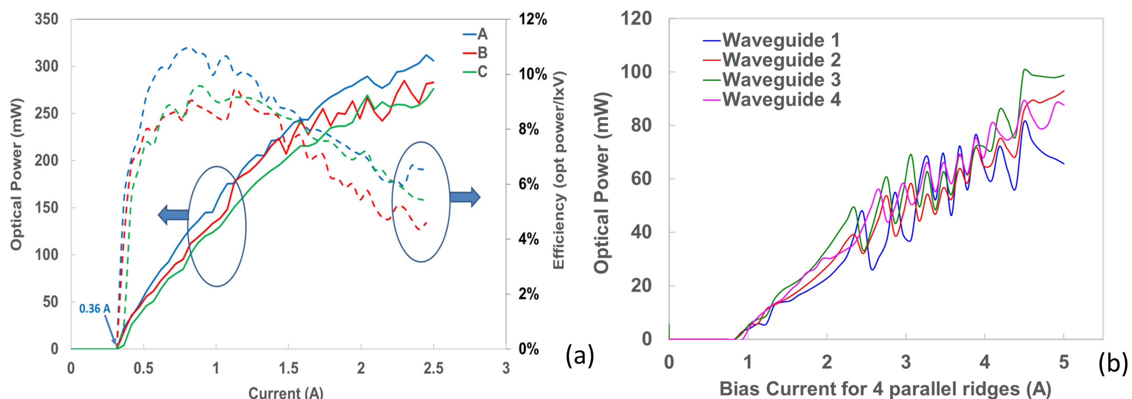

Fig. 5. (a) Power vs current (L-I) and electrical efficiency from three hybridized single-element InGaAsP/InP SCOECL devices biased up to 2.5A T = 25°C. The best-aligned of the three devices (A) emits 312 mW at 2.5A. (b) L-I plot for a 4-element SCOWECL device showing ~80 mW emitted for each waveguide channel at a bias of 1.25 A per SCOWA (5 A total)T = 25°C.

estimate that ~8 modes would be supported in the grating bandwidth. Mode hopping can potentially be mitigated with a compensating phase tuning section implemented using a thermal tuner in the SiNx WG between gain and DBR.

Optical spectra shown in Fig. 6(a) and 6(b) were obtained for the devices by collecting the laser output from the photonic submount output facet with a lensed fiber connected to an Agilent optical spectrum analyzer stepping at 0.04 nm. The optical spectra was collected at 2.2A for the single mode device and 2 A for the 4-element device. Optical spectra for the single element devices all show single longitudinal-mode operation with 55-dB side-mode suppression ratio (SMSR), and resolution limited linewidth emitting at 1538.6 nm. The left inset in Fig 6(a) shows a wider wavelength scan from 1440–1640 nm illustrates that no longitudinal sidemodes are visible (note the apparent saturation in the wide scan is an artifact of the step size sampling at higher rate than the amplitude resolution). The 4-channel devices show a lower 34 dB SMSR, limited by cross-coupling, which we hypothesize is a result of light leaking out of the bending SCOWA waveguides coupling through the waveguide slab to neighboring elements despite the 50 μm spacing of the array. Confirmation of this mechanism and approaches to mitigate the cross-coupling is currently under study. Mode images were collected by focusing the emission spot through an aspherical lens onto an IR camera. The emitted mode from the SiN waveguide was approximately 5 μm (width) $\times$ 4 μm (height) ($1/e^2$). The mode images of the single and 4-element devices from the SiN-waveguide outputs are also shown as insets in Figs. 6(a) and (b).

Relative intensity noise (RIN) and frequency noise were measured for the three single-element SCOWECL's under 1-A bias conditions. Photocurrent was measured using a low-noise high-bandwidth InGaAs photodiode (Discovery Semiconductor DSC 30S) and a high-frequency vector signal analyzer (Agilent E4440A). The measured RIN spectra Fig. 7(a), are shot-noise limited (~−160 dB/Hz) from 1–20 GHz offset frequency and less than −140 dB/Hz down to 100 MHz. Frequency noise data were collected using the Mach-Zehnder interferometer method [17], [18] with an optical fiber delay line that was 26 m in length. A plot of a representative frequency-noise spectrum collected with 1 A bias for Device C is shown in Fig. 7(b). Analysis of this spectrum reveals integrated and Lorentzian linewidths of 192 kHz and 8 kHz, respectively [19]. The fundamental line width of 8 kHz presented in this study is broader than that reported by others [5], [12], and is not fully understood, but may arise from mode competition within the cavity.

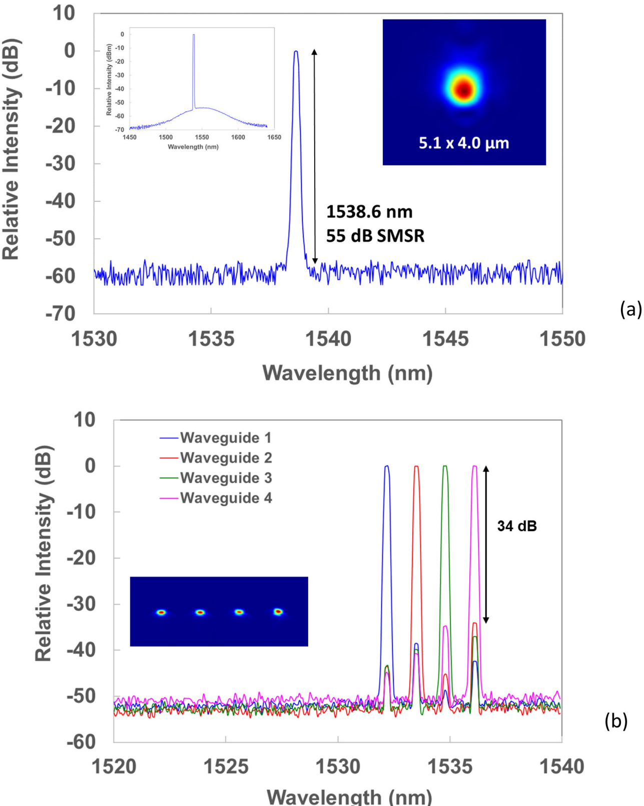

Fig. 6. (a) Optical spectrum of single-element SCOWECL A, showing single longitudinal-mode emission with 55 dB SMSR at 2.2A bias. The left inset image shows a wide wavelength scan showing that no other lasing peaks are visible from 1440–1640 nm. (b) Optical spectra of a 4-element emitter biased at 2.0 A coupled to 4 waveguides with 0.5 nm pitch variation on the DBR gratings creating ∼1 nm wavelength off-sets in the emission spectrum. Insets on both figures show the mode image captured by focusing the emission from the PIC output facet through an aspherical lens onto an Infra-red camera.

3.2 Coupling Loss Measurement

An estimate of the coupling loss between the SiN PIC waveguide and flip-chip bonded SCOWA device was obtained by operating the SCOWA devices in reverse bias as photodetectors. The photodiode responsivity of several non-hybridized reference SCOWAs was measured by coupling a 1550-nm laser source through a lensed PM fiber into the SCOWA devices reverse biased at 1.5 V. The responsivity of hybridized SCOWECL laser devices were similarly measured with input fiber being coupled to the SiN waveguide of the photonic submount chip facet. The ratio of the responsivity of the hybridized SCOWECLs and the reference SCOWA devices was then interpreted as the coupling efficiency. This estimate of coupling efficiency includes the following assumptions: (i) the responsivity of the hybridized and non-hybridized SCOWA devices is nominally the same, and (ii) the lensed-fiber-to-SCOWA and lensed-fiber-to-SiN-waveguide coupling loss are the same. We tested 8 SCOWECL devices (4 each of the single, and 4-element variants) and obtained an estimated coupling loss of −1.6 +/−1.0 dB. Fig. 8 shows the laser power at 2.5-A forward bias and estimated coupling loss vs. lateral misalignment of the flip chip device. This misalignment was measured by IR microscope inspection of SCOWA-to-PIC overlay Vernier alignment fiducials described in Section 2.3.

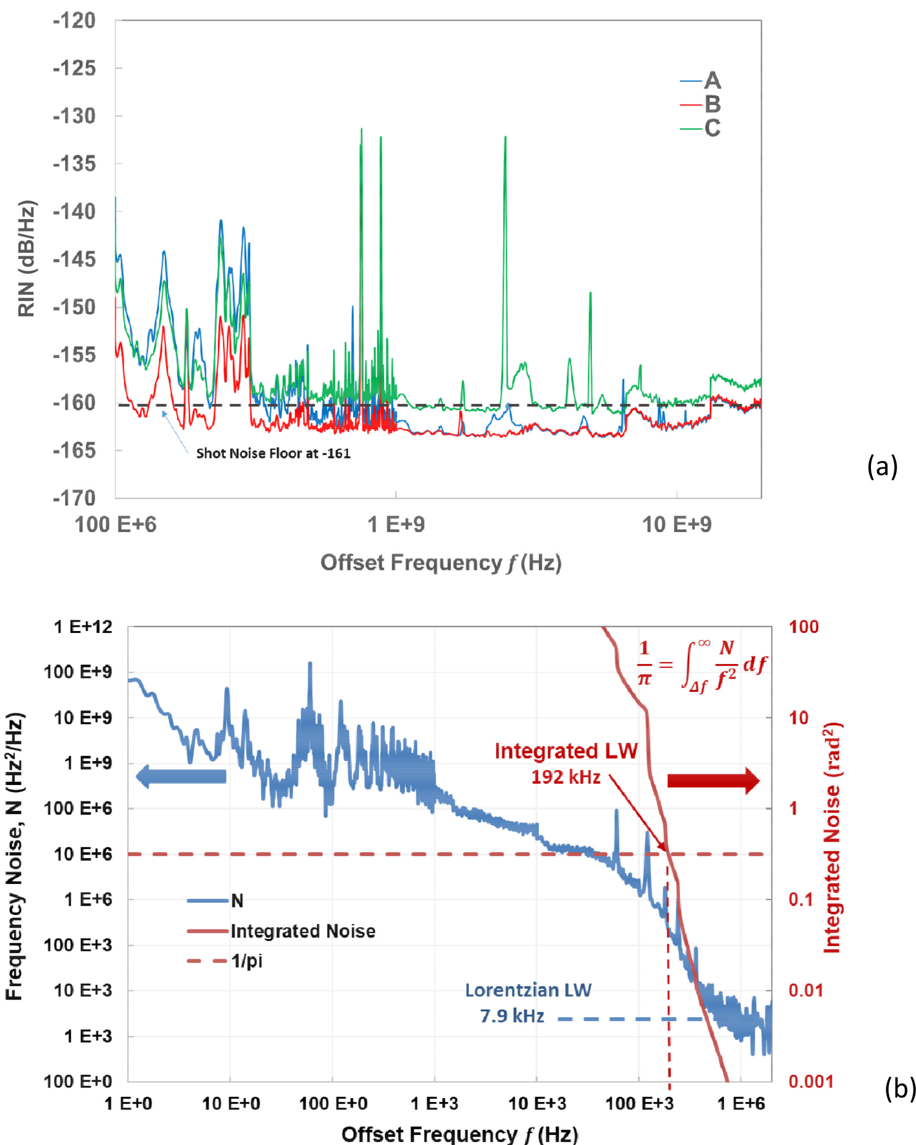

Fig. 7 (a) Relative intensity noise (RIN) spectra for external cavity lasers A,B & C showing shot-noise limited performance of <-160 dB/Hz from 1–20 GHz. (b) Measured frequency noise spectrum of a SCOWECL (Dev C) biased at 1.0 A with an integrated and Lorentzian linewidths of 192 kHz and 7.9 kHz, respectively.

3.3 Coupling Loss Analysis

The measured coupling loss between the SiN PIC and SCOWA devices was compared to coupling loss estimates extracted from a finite-difference time-domain (FDTD) simulation of the SiN-waveguide PIC submount and SCOWA structure. These simulations were performed using the Lumerical FDTD simulation tool. This model was focused on propagation across the coupling region with the transition from the SCOWA, across the air gap, and into an oxide clad SiN waveguide tip. A separate model investigated propagation loss in the 500 μm long linear taper and found it to be very low, in the range 0.015 dB. The coupling loss FDTD model features a SiN waveguide taper tip embedded in a 10-μm-tall and 20-μm-wide silicon dioxide cladding coupled to a SCOWA device with a structure described in Sec. 2.2. The III-V waveguide was angled at 5 degrees

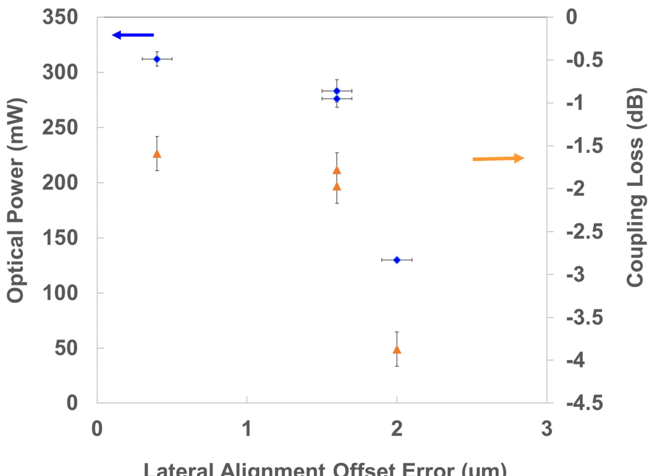

Fig. 8. Plot of optical power of single element SCOWECL devices biased at 2.5 A (T = 25.0°C) and coupling loss plotted against the measured lateral off-set position as determined from IR microcsopy of overlay Vernier alignment fiducials at the device bond interface.

and the receiving SiN waveguide angled at 11.3 degrees for optimal coupling. A variable-width air gap separated the III-V device from SiN PIC portion. An air gap was also included above the oxide cladding of the SiN PIC and below the SCOWA flipped surface. The facet of the SiN PIC is modeled with a 2° off-vertical angle, which is typical of the oxide etch process in the fabricated devices. The silicon substrate was omitted from the model since it has minimal influence on the optical mode. Coupling loss was calculated from the simulation by (i) launching the fundamental SCOWA mode in the III-V waveguide, (ii) propagating it across the air gap and into the SiN waveguide, and (iii) computing the overlap integral of the propagated energy with the SiN waveguide mode. The sensitivity of coupling loss to misalignment between waveguides was extracted from the model by sweeping the lateral and vertical position of SiN waveguide relative to III-V waveguide. Additionally, the impact of the air-gap width (*i.e.*, stand-off distance between the SCOWA and SiN PIC), and the width of SiN waveguide taper on coupling were examined. Fig. 9 shows a diagram of the Lumerical model, and the solved transverse modes for the SiN waveguide taper and SCOWA.

The simulated SCOWA near-field transverse mode profile and dimensions Fig. 9(b) agreed well with the mode profile measured using a collection lens and IR camera. The transverse mode profile at the output of the SiN-waveguide inverse taper was also modeled for various taper-termination widths ranging from 0.25 μm to 0.5 μm. Mode profiles calculated for a 0.45-μm width taper (fabricated width) were found to have a 1/e^2 width of about 2 μm, which is approximately $\sim$2 μm smaller than measured. Top oxide cladding thickness in the range of 2–5 μm used on this device was also found to not have a strong impact on the mode size and coupling efficiency. The root cause of the discrepancy in the measured vs modeled beam widths in SiN taper is still under investigation. It may be related to the highly evanescent nature of the mode in the taper not being accurately captured by a 1/e^2 mode width metric, but may be better represented by a 2nd moment or 95% energy integral width measure. The calculated 1/e^2 mode dimensions from a 0.3-μm taper width were $\sim$3.7 μm $\times$ 4.8 μm (Fig 9(c)), which agreed much more closely with the $\sim$4 $\times$ 5 μm mode measured in near field from the fabricated devices (Fig 6a). Since the 0.3-μm taper width generated a mode of similar size to that measured, this width was utilized in the model for estimating coupling loss.

Coupling efficiency was found to be relatively insensitive to variation in the gap between the III-V and SiN waveguides, with $<$0.5 dB loss for the 0–2.5 μm gaps evaluated. Coupling was also relatively insensitive to vertical misalignment, showing $<$0.5 dB change in coupling for $+/-1$ μm vertical waveguide positional variation. The largest source of coupling sensitivity was found to

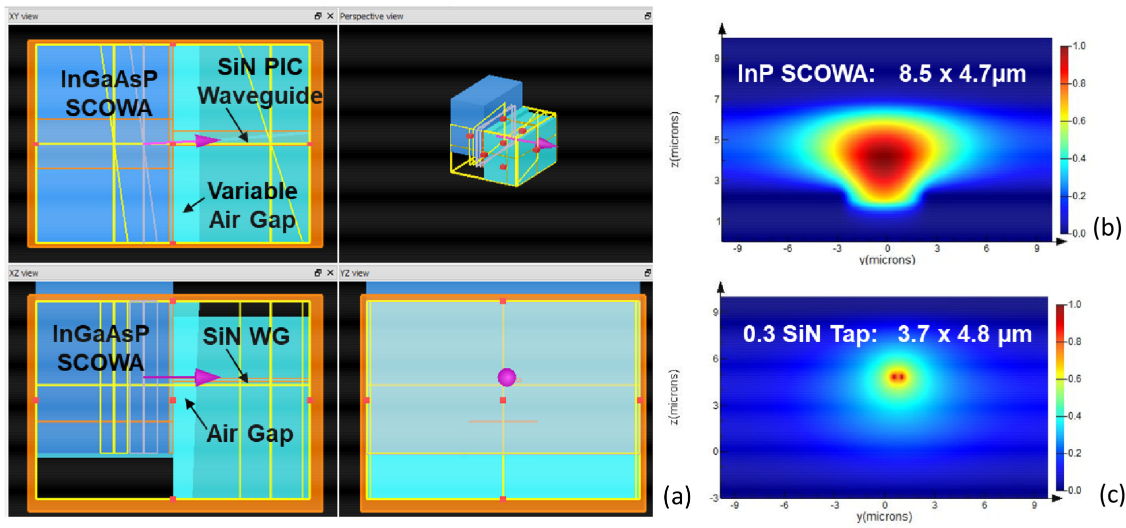

Fig. 9. (a) Lumerical FDTD model of SCOWA to SiN PIC coupling, and calculated modes for the (b) SCOWA and (c) 0.3-μm SiN taper tip.

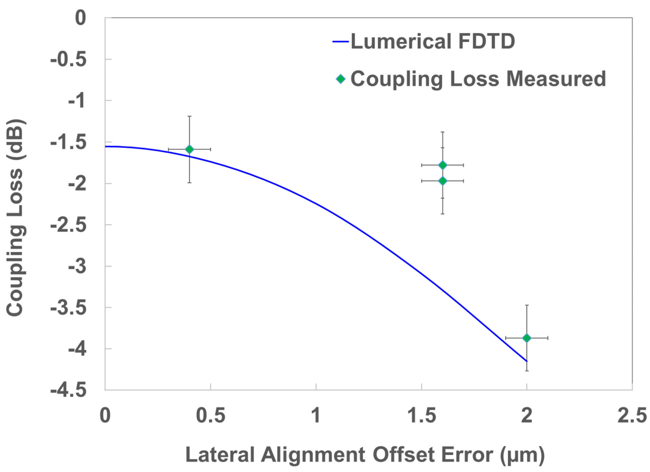

Fig. 10. Plot of measured (symbols) and simulated (solid line) coupling loss from four single-element SCOWECLs, as a function of lateral positional alignment between the SCOWA and SiN waveguides.

be lateral misalignment between SCOWA and SiN modes. The higher sensitivity to lateral vs. vertical misalignment is attributed to the presence of angled SCOWA and SiN waveguides in the lateral direction. Fig. 10 compares the measured coupling loss from the SCOWECL devices to that derived from the Lumerical simulation plotted against the lateral position of the devices as determined from IR microscopy of the overlay Vernier marks. Relatively good agreement is achieved between the modeled and measured coupling loss magnitude and its dependence on the measured lateral offset error. However, this comparison is limited by the small sample size in these initial experiments. A low coupling loss of -2 dB was measured for two devices (B, C), despite a lateral shift of 1.6 μm, a value better than predicted by the Lumerical model. For the Vernier fiducials, the measurement error based on resolution of optimal Vernier alignment is on the order of 0.2 μm. The coupling loss measurement error is estimated at 0.4 dB, based on variation in the reference device photocurrent baseline. The source of the deviation of these points from the modeled trend is larger than we expect based on the estimates of measurement error, and the root

cause remains under investigation. The low coupling loss achieved supports the use of dilute SiN waveguides for coupling to large mode SCOWA devices. Future work aims to better understand avenues for further improving the coupling loss perhaps by engineering tapers that provide for improved mode matching.

4. Conclusion

We reported the fabrication and performance of hybrid-integrated double-pass InGaAsP/InP SCOWAs structures passively aligned and flip-chip bonded into a slot on a PIC containing a low loss SiN waveguide DBR grating having 20% reflectivity. The resulting high optical power SCOWECL emits 312 mW at 2.5-A bias current, which we believe is the highest reported for a hybrid integrated external-cavity laser. The device exhibits a threshold of 360 mA, a 10% photon conversion efficiency, and a 55-dB SMSR. Additionally, we demonstrated flip-chip bonding and coupling of a 4-element SCOWA array to four waveguide DBRs, resulting in a multi-wavelength SCOWECL producing 80 mW per channel at a bias of 1.25 A/channel. We estimated the SCOWA-to-SiN-waveguide coupling loss to be $\sim$1.6 $+/-$1.0 dB, which agrees well with our FDTD simulation.

References

[1] C. Sorace-Agaskar *et al.*, “Versatile silicon nitride and alumina integrated photonic platforms for the ultraviolet to short-wave infrared,” *IEEE J. Quantum Electron.*, vol. 25, no. 5, Sep./Oct. 2019, Art. no. 8201515.

[2] G. Roelkens, D. Van Thourhout, R. Baets, R. Nötzel, and M. Smit, “Laser emission and photodetection in an InP/InGaAsP layer integrated on and coupled to a Silicon-on-Insulator waveguide circuit,” *Opt. Exp.*, vol. 14, pp. 8154–8159, 2006.

[3] A. W. Fang, H. Park, O. Cohen, R. Jones, M. J. Paniccia, and J. E. Bowers, “Electrically pumped hybrid algainas-silicon evanescent laser,” *Opt. Exp.*, vol. 14, pp. 9203–9210, 2006.

[4] T. Aihara *et al.*, “Membrane buried-heterostructure DFB laser with an optically coupled III-V/Si waveguide,” *Opt. Exp.*, vol. 27, pp. 36438–36448, 2019.

[5] D. Huang *et al.*, “High-power sub-kHz linewidth lasers fully integrated on silicon,” *Optica*, vol. 6, pp. 745–752, 2019.

[6] A. Malik, J. Guo, M. A. Tran, G. Kurczveil, D. Liang, and J. E. Bowers, “Widely tunable, heterogeneously integrated quantum-dot O-band lasers on silicon,” *Photon. Res. Vol.*, vol. 8, pp. 1551–1557, 2020.

[7] H. Guan *et al.*, “Widely-tunable, narrow-linewidth III-V/silicon hybrid external-cavity laser for coherent communication,” *Opt. Exp.*, vol. 26, no. 7, pp. 7920–7933, 2018.

[8] M. Theurer *et al.*, “Flip-Chip integration of InP to SiN photonic integrated circuits,” *J. Lightw. Technol.*, vol. 38, no. 9, pp. 2630–2636, 2020.

[9] P. A. Morton and M. J. Morton, “High-Power, ultra-low noise hybrid lasers for microwave photonics and optical sensing,” *J. Lightw. Technol.*, vol. 36, no. 21, pp. 5048–5057, 2018.

[10] S. Tanaka *et al.*, “High-power flip-chip-bonded silicon hybrid laser for temperature-control-free operation with micro-ring resonator-based modulator,” in *Proc. SPIE 8630, Optoelectron. Interconnects XIII*, 2013, Art. no. 86300Q.

[11] C. Xiang, P. A. Morton, and J. E. Bowers, “Ultra-narrow linewidth laser based on a semiconductor gain chip and extended Si3N4 bragg grating,” *Opt. Lett.*, vol. 44, pp. 3825–3828, 2019.

[12] Y. Fan *et al.*, “Hybrid integrated inp-Si3N4 diode laser with a 40-Hz intrinsic linewidth,” *Opt. Exp.*, vol. 28, pp. 21713–21728, 2020.

[13] van Rees *et al.*, “Realization of a hybrid integrated diode laser for visible light,” in *Proc. 22nd Eur. Conf. Integr. Opt. (ECIO)*, Paris, France, 2020.

[14] D. T. Spencer, M. Davenport, S. Srinivasan, J. Khurgin, P. A. Morton, and J. E. Bowers, “Low kappa, narrow bandwidth Si3N4 bragg gratings,” *Opt. Exp.*, vol. 23, pp. 30329–30336, 2015.

[15] P. W. Juodawlkis *et al.*, “High-Power, low-noise 1.5-μm slab-coupled optical waveguide (SCOW) emitters: Physics, devices, and applications,” *IEEE J. Quantum Electron.*, vol. 17, no. 6, pp. 1698–1713, Nov./Dec. 2011.

[16] J. N. Walpole *et al.*, “Slab-Coupled 1.3-μm semiconductor laser with single-spatial large-diameter mode,” *IEEE Photon. Tech. Lett.*, vol. 14, no. 6, pp. 756–758, Jun. 2002.

[17] Z. Zhang and A. Yariv, “A general relation between frequency noise and lineshape of laser light,” *IEEE J. Quantum Electron.*, vol. 56, no. 3, pp. 1–5, Jun. 2020.

[18] O. Llopis, P. H. Merrer, H. Brahimi, K. Saleh, and P. Lacroix, “Phase noise measurement of a narrow linewidth CW laser using delay line approaches,” *Opt. Lett.*, vol. 36, pp. 2713–2715, 2011.

[19] D. R. Hjelme, A. R. Mickelson, and R. G. Beausoleil, “Semiconductor laser stabilization by external optical feedback,” *IEEE J. Quantum Electron.*, vol. 27, no. 3, pp. 352–372, Mar. 1991.